Journal of Advanced Ceramics
2019, **8**(1): 148–152
https://doi.org/10.1007/s40145-019-0319-3
ISSN 2226-4108
CN 10-1154/TQ

Rapid Communication

A high entropy silicide by reactive spark plasma sintering

Yuan QIN[a], Ji-Xuan LIU[a], Fei LI[a], Xiaofeng WEI[a],
Houzheng WU[b], Guo-Jun ZHANG[a,*]

[a]*State Key Laboratory for Modification of Chemical Fibers and Polymer Materials*, *Institute of Functional Materials*, *College of Materials Science and Engineering*, *Donghua University*, *Shanghai 201620*, *China*
[b]*Department of Materials*, *Loughborough University*, *Leicestershire LE11 3TU*, *United Kingdom*

Received: February 15, 2019; Accepted: February 18, 2019

Abstract: A high-entropy silicide (HES), $(Ti_{0.2}Zr_{0.2}Nb_{0.2}Mo_{0.2}W_{0.2})Si_2$ with close-packed hexagonal structure is successfully manufactured through reactive spark plasma sintering at 1300 ℃ for 15 min. The elements in this HES are uniformly distributed in the specimen based on the energy dispersive spectrometer analysis except a small amount of zirconium that is combined with oxygen as impurity particles. The Young's modulus, Poisson's ratio, and Vickers hardness of the obtained $(Ti_{0.2}Zr_{0.2}Nb_{0.2}Mo_{0.2}W_{0.2})Si_2$ are also measured.

Keywords: high-entropy ceramics; high-entropy silicide; spark plasma sintering; silicide

1 Introduction

As a large class of materials, metal silicides have been widely studied aiming for applications as high-temperature oxidation resistant coatings, integrated circuit electrode films and other functional materials because of their excellent high-temperature oxidation resistance and electrical and thermal conductivity. Among these silicides, probably the most known one is molybdenum disilicide ($MoSi_2$), which has been widely used as resistive heating elements up to 1800 ℃ in air and manufactured in an industry scale for decades [1–4]. Through alloying, $MoSi_2$-based composites become very promising for structural components used at high temperatures. It was found that by adding alloying elements into $MoSi_2$, the room temperature toughness was improved and pest phenomena reduced [5]. Zhang *et al*. [6] later reported that the formation of $Mo(Si,Al)_2$ through adding aluminium significantly improved the mechanical properties of $MoSi_2$. Alman and Govier [7] manufactured a $Mo(Si,Al)_2$ alloy through hot-pressing, showing reduced or even eliminated pest phenomenon. $MoSi_2$ can be reinforced by secondary ceramic particles, whiskers or fibers, in order to improve its high temperature creep resistance and room temperature toughness. The reported successful examples include: $Mo(Si_{1-x}Al_x)_2$ reinforced by SiC particles manufactured through reactive sintering [8], $MoSi_2$-based composites with TiB_2, ZrB_2, HfB_2, and SiC as secondary particles through external mixing process [9].

In recent years, high-entropy alloys (HEAs), also known as multi-principal element alloys have attracted researchers' attention [10]. HEAs are defined as those composed of five or more principal elements in equal molar or near-equal ratios and a single-phase solid solution formed with simple lattice structures (such as BCC or FCC) [11,12]. With performance considered,

* Corresponding author.
E-mail: gjzhang@dhu.edu.cn

HEAs demonstrate excellent mechanical properties, corrosion resistance, thermal properties, and radiation resistance when compared to conventional materials [13–15].

So far, most research in this field focuses on metallic alloys. In recent years, however, attention has been attracted to high-entropy ceramics (HECs). The as-manufactured HECs have demonstrated low thermal conductivity [16], excellent oxidation resistance [17], good corrosion resistance [18], resistance to extreme heat, etc., strongly depended on the composition and structure of a HEC [19,20]. It has been proposed that significant lattice distortion would exist in HECs owing to the intrinsic atomic disorder of metal elements [21,22].

Rost *et al*. [23] reported a single-phase rock salt structured $(Mg_{0.2}Co_{0.2}Ni_{0.2}Cu_{0.2}Zn_{0.2})O$ high-entropy oxide prepared by quenching process. The oxide and its derivative $(Mg_{0.2}Co_{0.2}Ni_{0.2}Cu_{0.2}Zn_{0.2})_{1-x-y}A_xGa_yO$ (A = Li, Na or K), exhibit great dielectric constant and superior conductivity [24]. High-entropy borides such as $(Hf_{0.2}Zr_{0.2}Ta_{0.2}Nb_{0.2}Ti_{0.2})B_2$ and $(Hf_{0.2}Zr_{0.2}Ta_{0.2}Mo_{0.2}Ti_{0.2})B_2$ were prepared via SPS [22]. High-entropy carbide $(Hf_{0.2}Zr_{0.2}Ta_{0.2}Nb_{0.2}Ti_{0.2})C$ synthesized from individual carbide powders demonstrates lower thermal diffusivity and conductivity when compared to the binary carbides from such as HfC, ZrC, TaC, and TiC [16].

However, there is no open literature on the study of high-entropy silicides. In this article, we report a high-entropy silicide ceramic (HES) prepared via reactive spark plasma sintering (R-SPS), and its mechanical properties were characterized in a preliminary fashion.

2 Experimental

$(Ti_{0.2}Zr_{0.2}Nb_{0.2}Mo_{0.2}W_{0.2})Si_2$ HES was prepared via R-SPS based on the following general reaction:

$$0.2Ti + 0.2Zr + 0.2Nb + 0.2Mo + 0.2W + 2Si \rightarrow \left(Ti_{0.2}Zr_{0.2}Nb_{0.2}Mo_{0.2}W_{0.2}\right)Si_2$$

Each element of Ti, Zr, Nb, Mo, and W can react with Si at room temperature or above with high heat released according to thermodynamic calculation. The elements of titanium (Zr, 99.6%, 45 μm), zirconium (Zr, 99.7%, 45 μm), niobium (Nb, 99.95%, 45 μm), molybdenum (Mo, 99.6%, 45 μm), tungsten (W, 99.6%, 0.8 μm) and silicon (Si, 99.6%, 45 μm) were used as starting powders. The mixture of these powders with a composition ratio of 0.2 mole fraction in each mole of disilicide for the ended HES were mixed in a planetary ball mill for 12 hours using Si_3N_4 balls and ethanol as the mixing media. The as-prepared powder mixtures were loaded into graphite dies, then SPS was performed in a furnace (FCT, KCE®-FCT H-HP D 250, Germany) at different temperatures ranging from 900 to 1300 ℃ for 5 min under a pressure of 30 MPa. For obtaining denser HES, SPS with a dwelling time of 10 and 15 min at 1300 ℃ was also tried. The heating rate for all samples was set as 100 ℃/min, and cooling after sintering was complete in a natural manner without control after shutting down the heating power.

The phase composition of the as-sintered sample was characterized by XRD using Cu Kα radiation. The microstructures and element distributions in the obtained specimens were characterized with field emission scanning electron microscope (FE-SEM, Hitachi S-4800) attached with energy dispersive spectroscopy (EDS) probe. The residual oxygen content in the high-entropy silicide was tested by an oxygen/nitrogen analyzer (TC600C, Leco, USA).

The density of the as-sintered samples was measured by using the Archimedes method. Theoretical density of the HES was calculated based on the crystal structure and lattice parameters measured from XRD of the sample SPSed at 1300 ℃ for 15 min. Young's modulus was evaluated by advanced ultrasonic material characterization system (UMS-100, France). Vickers hardness (*H*v) was measured on as-polished surface under a load of 1 kg with a dwell time of 5 s, at least 10 measurements were conducted to get the average values.

3 Results and discussion

Figure 1 shows the XRD patterns of the samples SPSed at 900, 1100 and 1300 ℃ for 5 min and 1300 ℃ for 15 min. At temperature as low as 900 ℃, $(Mo,W)Si_2$ solid solution and ZrSi started to form, but elemental Si, Ti, Nb, and W were detectable. This fact evidences that the formation of HES is not a one-step process. With the sintering temperature increased to 1100 ℃, diffraction peaks of $NbSi_2$, $ZrSi_2$, and $TiSi_2$ appear while diffraction peaks of Si become weakened. After SPSed at 1300 ℃ for 5 min, single phase HES with hexagonal closest packed structure was formed. Accordingly, we can conclude that during the SPS process mono-silicides and disilicides were the intermediate phases formed at low temperatures and

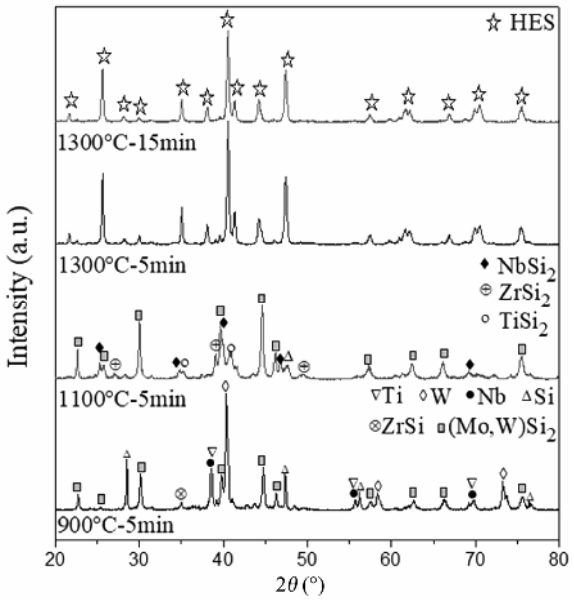

Fig. 1 XRD patterns of the samples SPSed at 900, 1100, and 1300 ℃ for 5 min and 1300 ℃ for 15 min.

the HES was formed at higher temperatures from these intermediate phases via a solid solution process. With the holding time extended from 5 to 15 min, the sample still maintained a single HES phase. The density of the specimen SPSed at 900 ℃ is only 2.80 g/cm^3. When the sintering temperature reaches 1100 ℃, the density increased to 5.23 g/cm^3. The densities of the samples with single-phase HES SPSed at 1300 ℃ with a holding time 5 and 15 min are 6.09 and 6.22 g/cm^3, respectively. It indicates that a densification process occurred during the later part of SPS after the single-phase HES was formed. Therefore, we chose the samples sintered at 1300 ℃ for 15 min for further characterization, and the results are shown below.

The lattice parameters of this HES phase is 4.653 Å for a and 6.511 Å for c, which is close to those for β-$MoSi_2$, as shown in Table 1. We use these lattice parameters to estimate the theoretical density of the as-formed HES, giving a density of 6.28 g/cm^3. Hence, a relative density of the as-sintered HES sample is ~99%. It is noteworthy that the β phase of $MoSi_2$, is stable only at high temperatures over 1900 ℃ [25], and the fact that similar phase appeared in a much lower synthesized temperature may be attributed to the formation of high-entropy phase, providing an extra thermodynamic stability at lower temperatures.

The SEM images of the polished surface of the $(Ti_{0.2}Zr_{0.2}Nb_{0.2}Mo_{0.2}W_{0.2})Si_2$ HES and the corresponding EDS mapping of Ti, Zr, Nb, Mo, W, and Si elements are shown in Fig. 2. It shows that the HES is dense without visible pores. Some impurity particles are

Table 1 Space group and lattice parameters of $(Ti_{0.2}Zr_{0.2}Nb_{0.2}Mo_{0.2}W_{0.2})Si_2$ HES and the corresponding individual silicides

Material	Space group	Lattice parameter (Å)		
		a	*b*	*c*
$(Zr_{0.2}Ti_{0.2}W_{0.2}Mo_{0.2}Nb_{0.2})Si_2$	$P6_222$(180)	4.653	4.653	6.511
β-$MoSi_2$ (stable>1900 ℃)	$P6_222$(180)	4.596	4.596	6.550
α-$MoSi_2$ (stable<1900 ℃)	*I*4/*mmm*(139)	3.205	3.205	7.845
$NbSi_2$	$P6_222$(180)	4.797	4.797	6.592
$ZrSi_2$	*Cmcm*(63)	3.396	14.751	3.665
$TiSi_2$	*Cmcm*(63)	3.620	13.760	3.605
WSi_2	*I*4/*mmm*(139)	3.211	3.211	7.829

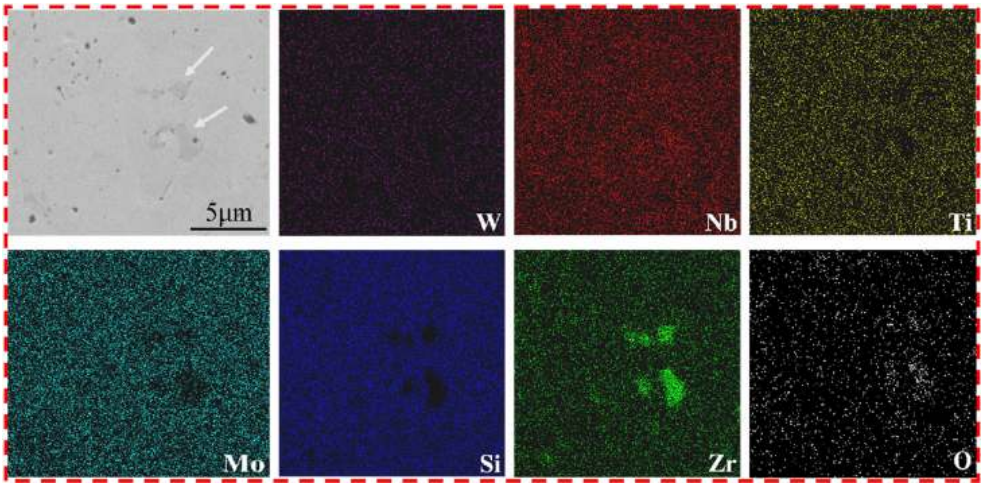

Fig. 2 SEM images of the polished surface of $(Ti_{0.2}Zr_{0.2}Nb_{0.2}Mo_{0.2}W_{0.2})Si_2$ SPSed at 1300 ℃ for 15 min, with the corresponding EDS mapping of Ti, Zr, Nb, Mo, W, and Si elements.

noted, as arrowed in Fig. 2. The distributions of these metal elements except Zr are homogeneous at this resolution. The arrowed particles show Zr enriched. EDS map of oxygen was also acquired, showing that oxygen enrichment appeared in Zr-enriched regions. The measured oxygen content of the specimen is 1.50 wt%. As per this fact, we assume that zirconium might have acted as getter of impurity oxygen in this system, as oxygen contamination exists unavoidably in the starting metal powders or during the processing.

The SEM micrograph of the fracture surface of the HES is shown in Fig. 3. The fracture micrograph of the sample reveals that the fracture mode is transgranular dominated. The average grain size of the sample is about 4 μm.

The Young's modulus and Poisson's ratio of the as-manufactured HES ceramic are 352 GPa and 0.32 respectively, and the measured Vickers hardness (*H*v) is 12.09 GPa. The hardness seems to be in the range between upper and lower bound of reported values of the disilicides by different researchers [4,26–30]. For example, the Vickers hardness of $MoSi_2$ [27], $NbSi_2$ [28], WSi_2 [29], and $TiSi_2$ [30] are 10.5, 8.76, 13.75, and 8–10 GPa, respectively. For some metal–silicon binary systems such as Zr–Si, there exist several silicides with different elemental ratios of Zr to Si, and it is difficult to prepare a mono-phase material [31], making it difficult to evaluate properties of these phases. As discussed in very recent publications [20, 21,32], the hardness of HECs is higher than the corresponding mono-compositional ceramics, i.e., the mixture rule fails to apply. It is premature, however, for us to make similar conclusion. Mechanisms responsible for hardness enhancement in high-entropy materials can be dictated by electronic valency inside the phase, solid solution strengthening, and Hall–Petch effect related to grain size at microstructure level. For HES, more comprehensive characterization is needed to confirm if hardening exists and what the possible mechanism is responsible for any hardening. Other properties of the obtained $(Ti_{0.2}Zr_{0.2}Nb_{0.2}Mo_{0.2}W_{0.2})Si_2$ HES such as oxidation resistance, as well as other high-entropy silicides with different metal elemental compositions are under investigation.

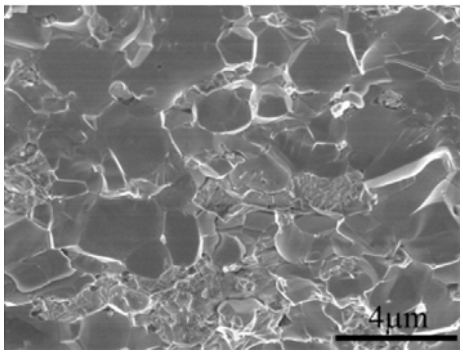

Fig. 3 SEM photograph of fracture surface of $(Ti_{0.2}Zr_{0.2}Nb_{0.2}Mo_{0.2}W_{0.2})Si_2$ HES SPSed at 1300 ℃ for 15 min.

4 Conclusions

In this work, a high-entropy silicide (HES), $(Ti_{0.2}Zr_{0.2}Nb_{0.2}Mo_{0.2}W_{0.2})Si_2$ was successfully synthesized by spark plasma sintering from element raw materials. The crystal structure identified by XRD is hexagonal closest packed. The elements except Zr are uniformly distributed in the HES based on the EDS analysis. A small amount of zirconium and oxygen enriched regions were detected as impurity due to the oxygen contamination in the raw materials and during the processing. For an as-manufactured HES with a relative density of 99%, its Young's modulus, Poisson's ratio, and Vickers hardness are 352 GPa, 0.32, and 12.09 GPa, respectively.

Acknowledgements

Financial support from the National Natural Science Foundation of China (Nos. 51532009 and 51872045), and the Science and Technology Commission of Shanghai Municipality (No. 18ZR1401400) are gratefully acknowledged.

References

[1] Petrovic JJ, Vasudevan AK. Key developments in high temperature structural silicides. *Mat Sci Eng A* 1999, **261**: 1–5.

[2] Shah DM, Berczik D, Anton DL, *et al*. Appraisal of other silicides as structural materials. *Mat Sci Eng A* 1992, **155**: 45–57.

[3] Petrovic JJ, Vasudevan AK. Overview of high temperature structural silicides. *Mater Res Soc Symp P* 1993, **322**: 3–8.

[4] Jeng YL, Lavernia EJ. Processing of molybdenum disilicide. *J Mater Sci* 1994, **29**: 2557–2571.

[5] Mckamey CG, Tortorelli PF, Devan JH, *et al*. A study of pest oxidation in polycrystalline $MoSi_2$. *J Mater Res* 1992, **7**: 2747–2755.

[6] Zhang GJ, Yue XM, Watanabe T. Synthesis of $Mo(Si,Al)_2$

alloy by reactive hot pressing at low temperatures for a short time. *J Mater Sci* 1999, **34**: 593–597.

[7] Alman DE, Govier RD. Influence of Al additions on the reactive synthesis of $MoSi_2$. *Scripta Mater* 1996, **34**: 1287–1293.

[8] Zhang GJ, Yue XM, Watanabe T, *et al*. In situ synthesis of $Mo(Si,Al)_2$–SiC composites. *J Mater Sci* 2000, **35**: 4729–4733.

[9] Cook J, Khan A, Lee E, *et al*. Oxidation of $MoSi_2$-based composites. *Mat Sci Eng A* 1992, **155**: 183–198.

[10] Yeh JW, Chen SK, Lin SJ, *et al*. Nanostructured high-entropy alloys with multiple principal elements: novel alloy design concepts and outcomes. *Adv Eng Mater* 2004, **6**: 299–303.

[11] Tsai MH, Yeh JW. High-entropy alloys: A critical review. *Mater Res Lett* 2014, **2**: 107–123.

[12] Yong Z, Zuo TT, Tang Z, *et al*. Microstructures and properties of high-entropy alloys. *Pros Mater Sci* 2014, **61**: 1–93.

[13] Miracle DB, Senkov ON. A critical review of high entropy alloys and related concepts. *Acta Mater* 2017, **122**: 448–511.

[14] Egami T, Ojha M, Khorgolkhuu O, *et al*. Local electronic effects and irradiation resistance in high-entropy alloys. *Jom* 2015, **67**: 2345–2349.

[15] Granberg F, Nordlund K, Ullah MW, *et al*. Mechanism of radiation damage reduction in equiatomic multicomponent single phase alloys. *Phys Rev Lett* 2016, **116**: 135504.

[16] Yan XL, Constantin L, Lu YF, *et al*. $(Hf_{0.2}Zr_{0.2}Ta_{0.2}Nb_{0.2}Ti_{0.2})C$ high-entropy ceramics with low thermal conductivity. *J Am Ceram Soc* 2018, **101**: 4486–4491.

[17] Zhou JY, Zhang JY, Zhang F, *et al*. High-entropy carbide: A novel class of multicomponent ceramics. *Ceram Int* 2018, **44**: 22014–22018.

[18] Braic V, Balaceanu M, Braic M, *et al*. Characterization of multi-principal-element (TiZrNbHfTa)N and (TiZrNbHfTa)C coatings for biomedical applications. *J Mech Behav Biomed* 2012, **10**: 197–205.

[19] Hong QJ, Walle AVD. Prediction of the material with highest known melting point from *ab initio* molecular dynamics calculations. *Phys Rev B* 2015, **92**: 020104(R).

[20] Castle E, Csanádi T, Grasso S, *et al*. Processing and properties of high-entropy ultra-high temperature carbides. *Sci Rep-UK* 2018, **8**: 8609.

[21] Sarker P, Harrington T, Toher C, *et al*. High-entropy high-hardness metal carbides discovered by entropy descriptors. *Nat Commun* 2018, **9**: 4980.

[22] Gild J, Zhang YY, Harrington T, *et al*. High-entropy metal diborides: A new class of high-entropy materials and a new type of ultrahigh temperature ceramics. *Sci Rep-UK* 2016, **6**: 37946.

[23] Rost CM, Sachet E, Borman T, *et al*. Entropy-stabilized oxides. *Nat Commun* 2015, **6**: 8485.

[24] Bérardan D, Franger S, Dragoe D, *et al*. Colossal dielectric constant in high entropy oxides. *Phys Status Solidi* 2016, **10**: 328–333.

[25] Unal O, Petrovic JJ, Carter DH, *et al*. Dislocations and plastic deformation in molybdenum disilicide. *J Am Ceram Soc* 1990, **73**: 1752–1757.

[26] Liu GH, Li JT, Chen KX. Combustion synthesis of refractory and hard materials: A review. *Int J Refract Met H* 2013, **39**: 90–102.

[27] Kim HC, Park CD, Jeong JW, *et al*. Synthesis of dense $MoSi_2$ by high-frequency induction heated combustion and its mechanical properties. *Met Mater Int* 2003, **9**: 173–178.

[28] Ko IY, Kim BR, Nam KS, *et al*. Pulsed current activated combustion synthesis and consolidation of ultrafine $NbSi_2$ from mechanically activated powders. *Met Mater Int* 2009, **15**: 399–403.

[29] Oh DY, Kim HC, Yoon JK, *et al*. Synthesis of dense WSi_2 and WSi_2-*x*vol.% SiC composites by high-frequency induction heated combustion and its mechanical properties. *Met Mater Int* 2006, **12**: 307.

[30] Sonber JK, Murthy TSRC, Sairam K, *et al*. Effect of $TiSi_2$ addition on densification of cerium hexaboride. *Ceram Int* 2016, **42**: 891–896.

[31] Jérôme C, Jérôme Z, Julie B, *et al*. Composite zirconium silicides through an in situ process. *In J Appl Ceram Tec* 2006, **3**: 23–31.

[32] Harrington TJ, Gild J, Sarker P, *et al*. Phase stability and mechanical properties of novel high entropy transition metal carbides. *Acta Mater* 2019, **166**: 271–280.